

Artigo Original

Recebido em 06/01/2006 e aceito em 08/07/2006

Linear versus non-linear noninvasive temperature prediction in a homogeneous medium subjected to physiotherapeutic ultrasound

Comparação entre predição linear e não linear não-invasiva de temperatura num meio homogêneo sujeito a ultra-som de terapia

**César Alexandre Domingues Teixeira*,
Maria da Graça Cristo dos Santos Lopes
Ruano, António Eduardo de Barros
Ruano**

Centre for Intelligent Systems, Faculty of Sciences
and Technology, Campus de Gambelas, University of
Algarve, 8005-139 Faro, Portugal
E-mail: {cateixeira, mruano, aruano}@ualg.pt

Wagner Coelho Albuquerque Pereira

Biomedical Engineering Program – COPPE/UFRJ,
Bloco H, Caixa Postal 68510, Ilha do Fundão,
CEP 21941-972 Rio de Janeiro, Brazil
E-mail: wagner@peb.ufrj.br

Carlos Negreira

Laboratory of Ultrasound Acoustics,
Facultad de Ciencias, Universidad de la República,
Iguá 4225, Montevideo, 11400 Uruguay
E-mail: carlosn@fisica.edu.uy

*Corresponding author

Abstract

The lack of accurate time-spatial temperature estimators/predictors conditions the safe application of thermal therapies, such as hyperthermia. In this paper, a comparison between a linear and a non-linear class of models for non-invasive temperature prediction in a homogeneous medium, subjected to ultrasound at physiotherapeutic levels is presented. The linear models used were autoregressive with exogenous inputs (ARX) and the non-linear models were radial basis functions neural networks (RBFNN). In order to create and validate the models, an experiment was build to extract in vitro ultrasound RF-lines, as well as its correspondent temperature values. Then, features were extracted from the measured RF-lines and the models were trained and validated. For both the models, the best-fitted structures were selected using the multi-objective genetic algorithm (MOGA), given the enormous number of possible structures. The best RBFNN model presented a maximum absolute predictive error in the validation set five times less than the value presented by the best ARX model. In this work, the best RBFNN reached a maximum absolute error of 0.42 °C, which is bellow the value pointed as a borderline between an appropriate and an undesired temperature estimator, which is 0.5 °C. The average error was one order of magnitude less in the RBFNN case, and a less biased estimation was met. In addition, the best RBFNN needed less environmental information (inputs), given the capacity to non-linearly relate the information. The results obtained are encouraging, considering that coherent results should be obtained in a time-spatial modelling schema using RBFNN models.

Keywords: *Non-invasive temperature estimation, physiotherapeutic ultrasound, radial basis functions neural networks, multi-objective genetic algorithms.*

Resumo

A falta de estimadores de temperatura espaço-temporais que sejam precisos impede a aplicação segura das terapias térmicas, como por exemplo a hipertermia. Neste artigo é apresentada uma comparação entre uma classe de modelos lineares e uma classe de modelos não-lineares, na predição não invasiva de temperatura num meio homogêneo, quando o mesmo é aquecido por ultra-som em níveis usados em fisioterapia. Os modelos lineares considerados foram do tipo auto-regressivo com entradas exógenas (ARX); a nível não-linear foram considerados redes neuronais RBF (RBFNN). Para treinar e validar os modelos foram recolhidas as ecos provenientes do meio, bem como os correspondentes valores de temperatura. Após a colheita de informação, foram extraídas características dos ecos medidos e posteriormente os modelos foram treinados e validados. Para ambas as classes de modelos, as melhores estruturas foram seleccionadas usando um algoritmo genético multi-objectivo (MOGA), devido ao número elevado de estruturas possíveis. O melhor modelo RBFNN apresentou um erro máximo absoluto cinco vezes inferior ao erro máximo absoluto apresentado pelo melhor modelo ARX. Neste trabalho, o melhor modelo RBFNN apresentou um erro máximo absoluto de 0,42 °C, valor este que é inferior ao limite (0,5 °C) apresentado como sendo a fronteira entre um estimador desejado e um estimador indesejado. O erro médio cometido pelo melhor modelo neuronal é uma ordem de grandeza inferior ao erro médio apresentado pelo melhor modelo linear, obtendo-se deste modo uma estimacão menos enviesada no caso das redes neuronais, com menos informacão do ambiente (menos entradas) devido ao processamento não-linear dos dados de entrada. Os resultados obtidos são encorajadores, apontando no sentido de se obter bons resultados numa estimacão espaço-temporal.

Palavras-chave: Estimacão não-invasiva de temperatura, Fisioterapia por ultra-som, Redes neuronais RBF, Algoritmos genéticos multi-objectivo.

Introduction

Ultrasound as a therapeutic modality is commonly used for physiotherapy, hyperthermia, and surgery purposes (Ter Haar, 1999). Probably the most used one is the application of ultrasound as a way to heat tumours to cytotoxic temperatures (41-45 °C), in order to kill them or stop their growth. This technique is called hyperthermia, and was also pointed out as a viable complementation of chemotherapy and radiotherapy (Arthur *et al.*, 2005).

One of the aspects which restrain the application of thermal therapies is the lack of reliable and non-invasive temperature estimators in both time and space. Accurate time-spatial estimators/predictors would enable a correct therapy procedure by means of an appropriate therapeutic ultrasound instrumentation control. For hyperthermia purposes an accuracy of 0.5 °C in 1 cm³ is desired (Arthur *et al.*, 2005). Several works describing ways for non-invasively estimate the temperature have been published. Possible methods include electrical impedance tomography (Paulsen *et al.*, 1996), microwave radiometry (Meaney and Paulsen, 1996), magnetic resonance imaging (MRI) (Hynynen *et al.*, 1996) and backscattered ultrasound (BSU) (Arthur *et al.*, 2005; Seip and Ebbini, 1995; Simon *et al.*, 1998; Ueno *et al.*, 1990). From the above techniques, only MRI achieves the desired accuracy and spatial resolution. The disadvantages of MRI are its costs and the difficulty to use it in some thermal therapies (Arthur *et al.*, 2005).

The use of BSU brings some advantages, such as its non-ionizing property, low-cost and simple signal processing techniques required. Moreover, it can reach deep regions inside the body and have a good spatial and temporal localisation. BSU viability for non-invasive temperature estimation depends on measurable ultrasonic temperature-dependent parameters/features. In the work of Arthur *et al.* (2005), three categories of methods that use BUS for non-invasive estimation were pointed out: the ones that track the eco-shifts produced by changes in sound velocity and medium expansion, the ones that use the measurement of the attenuation coefficient, and those that measure the change in backscattered energy from tissue inhomogeneities. Actually, a fourth category exists that is based on tracking the frequency changes of the echo components (Seip and Ebbini, 1995). This variation is also due to the change in the speed of sound and in the medium expansion. Independently of the category, all methods assume that a linear relationship exists between the extracted ultrasonic parameters and the temperature.

In this work a comparison between a linear and a non-linear relationship involving the temperature in a homogeneous medium, and six spectral features and one temporal feature is proposed. The linear relationship was accomplished by means of an autoregressive model with exogenous inputs (ARX), while the non-linear modelling was performed by means of radial basis functions neural networks (RBFNNs). In both modelling strategies, the appropriate values of the structure variables were selected in a genetic multi-objective fashion by means of the multi-objective genetic algorithm (MOGA) (Fonseca and Fleming, 1993). The temperature-dependent features used in this work were applied with success in Teixeira *et al.* (2005) and Teixeira *et al.* (2006), thus the reason of its application in this work. In Teixeira *et al.* (2004) a comparison between the ARX and the RBFNN models was performed for invasive temperature estimation in a homogeneous medium. In the work of Teixeira *et al.* (2004), the models were trained for one step-ahead prediction, the RBFNNs inputs and number of neurons were selected by the MOGA while the ARX inputs were selected manually. In the present work, a more trustworthy comparison is proposed, where both the ARX inputs and RBFNN inputs and number of neurons are selected by the MOGA, in a non-invasive (as

required in a clinical environment) long-term (2 hours approximately) temperature prediction scheme.

Materials and Methods

The experimental setup used is presented in Figure 1.

In this figure, a reservoir containing 1,400 ml of glycerine can be seen, where three lead spheres (3 mm diameter) acting as scatterers are submerged. The glycerine medium with lead spheres was chosen having in mind the creation of a homogeneous medium with absorption compared to that of biological tissues, where a considerable heating can be reached, namely at the sphere/glycerine interface, with the intention to simulate a soft-tissue/bone interface. The glycerine heating changes its acoustical properties, namely the attenuation coefficient, and variations on the echo spectral amplitudes and bandwidth can be seen. The temperature change is also expressed in variations on speed of sound and medium expansion, which can be seen in the temporal position and central frequency changes of the echoes.

The temperature was measured at the central sphere using a type K thermocouple connected to a module with integrated cold junction compensation (Fluke 80TK). The medium was heated using an ultrasonic physiotherapeutic device (Ibramed Sonopulse

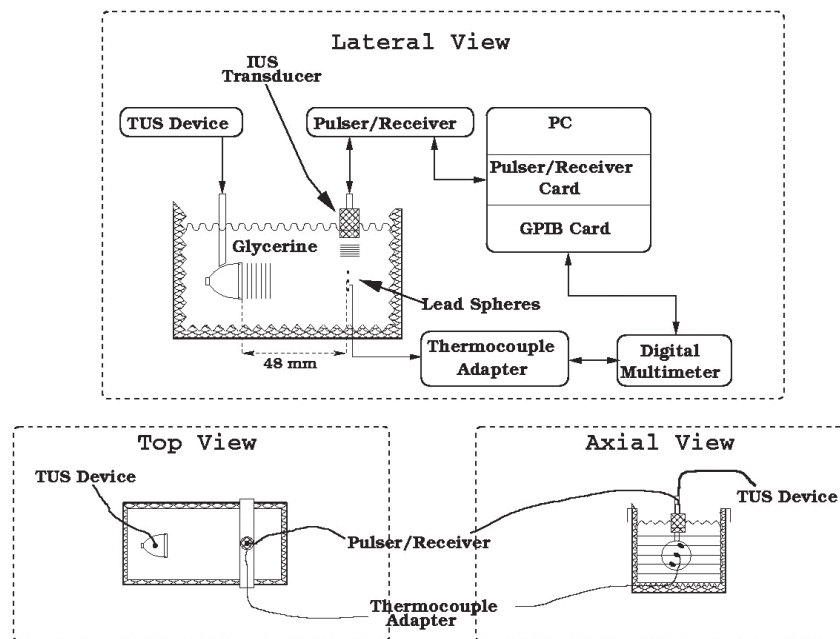


Figure 1. Experimental setup, viewed from the lateral, top and axial perspectives. The relative position between the therapeutic ultrasound (TUS) and the imaging ultrasound (IUS) transducer can be seen, as well as the positioning of the lead spheres.

Generation 2000, São Paulo, Brazil), working at 1 MHz with an effective radiation area of 3.5 cm². The therapeutic ultrasound (TUS) device heated the medium at three different intensities: 1, 1.5, and 2 W/cm² in continuous mode.

In order to perform a non-invasive temperature estimation trial, RF-lines were collected using an imaging ultrasound (IUS) transducer (Sonic, USA), driven by a PC controlled pulser/receiver (Corelec, France). The IUS transducer was a 5 MHz non-focused piston-like ultrasound transducer with a diameter of 1.27 cm. The IUS beam reached the spheres in a direction perpendicular to the TUS beam direction, avoiding the saturation of the imaging device. At each 10 seconds a complete RF-line (2,048 points, sampled at 40 MHz) was collected, as well as a temperature value, and saved for future features/parameters extraction. Each experiment lasted approximately 2 hours, where the glycerine was heated in the first hour, then the TUS beam was interrupted and the medium left to cool back to room temperature in the remaining hour. TUS intensity and frequency were kept constant in the heating hour. In the same way, the intensity and frequency of the IUS transducer were maintained constant during the entire 2-hour experiment. For each intensity, three data sets were saved, containing the temperature-RF-line pairs. The temperature ranges obtained are summarised in Table 1. As referred previously, the achievement of non-invasive temperature predictors require the computation of temperature-dependent features from the collected RF-lines. Since temperature measurement was only performed in the central sphere, feature extraction was only performed in the echo originated by this scatterer in conjunction with the thermocouple, in order to eliminate information from other regions of the medium where the temperature is unknown. After a boxcar window application, used to isolate the information, a fast Fourier transform (FFT) was employed and six spectral features computed. The spectral features were: the amplitude of the fundamental component originated

by the TUS device, located at approximately 1 MHz; the amplitude of the first and second harmonics of the fundamental component originated by the TUS beam, located at approximately 2 and 3 MHz, respectively; the amplitude, central frequency, and bandwidth (-6 dB) of the component originated by the IUS probe, which is located around the 5.5 MHz. The temporal feature extracted was the time position of the echo originated by the central scatterer, determined using the Hilbert Transform strategy. In a next step, the extracted features and the past temperature values were filtered using a causal low-pass Butterworth digital filter (order 1, cut-off frequency = 1/20 of the Nyquist frequency), and normalised to values between 0 and 1. The filter parameters were selected having in mind the noise reduction, maintaining fundamental behaviour of the signals. On the other hand, the normalisation was necessary to discard scales differences between the features. Both the two pre-processing tools were necessary to improve the training and structure selection of the models under study. At this point we have the following information for training, structure selection and validation: normalised and filtered amplitude of the fundamental component originated by the TUS beam – AF_{TUS} ; normalised and filtered amplitude of the first and second harmonics of the fundamental component originated by the therapeutic device – $AH1_{TUS}$ and $AH2_{TUS}$; normalised and filtered amplitude, central frequency and bandwidth of the component originated by the imaging device – A_{IUS} , F_{IUS} , and BW_{IUS} ; normalised and filtered temporal position – TP; and normalised and filtered temperature – T. In Figure 2, one example of the extracted features, as compared with the measured temperature is presented. Looking at this figure, it can be said that only TP, BW_{IUS} and F_{IUS} present some small linearity with the temperature. In general, the temperature was more precisely related with the extracted features by non-linear methods.

The past lags of the previously defined variables (AF_{TUS} , $AH1_{TUS}$, $AH2_{TUS}$, A_{IUS} , F_{IUS} , BW_{IUS} , TP, and T) were assigned as RBFNN and ARX inputs. In the

Table 1. Temperature ranges obtained for the three applied intensities. The maximum temperature is attained after a one-hour heating, while the final temperature is obtained at the end of the experiment, one hour after the TUS device was turned off.

Temperature (°C)	Intensity (W/cm ²)		
	1.0	1.5	2.0
Initial	28.3	24.5	28.2
Maximum	33.1	34.8	38.2
Final	29.2	28.3	31.2

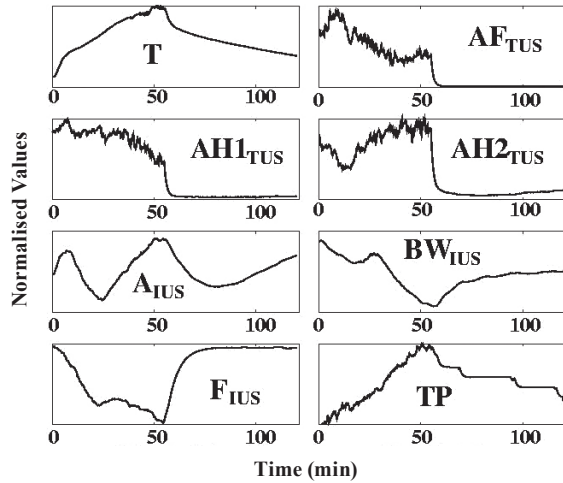


Figure 2. Extracted features from the measured RF-lines compared with the measured temperature (T). AFTUS: Amplitude of the fundamental component originated by the TUS beam. AH1TUS and AH2TUS: Amplitude of the first and second harmonics of the fundamental component originated by the therapeutic device. AIUS, FIUS, and BWIUS: Amplitude, central frequency and bandwidth of the component originated by the imaging device. TP: Temporal position.

framework used in this work and in the previous ones reported by the authors, three data sets are necessary: 1) a data set used for the computation of the model parameters, called the training set; 2) a data set used to access the models generalisation performance during the training and structure selection phases, called the test set; and 3) a third data set used to evaluate the best obtained models at the end of the training and structure selection phases, called the validation set. Having in mind the attainment of well-fitted models for the three applied intensities, the training set was formed by randomly selecting patterns from the three available sets (one for each intensity), 1/3 from each set. The complete data sequence collected at 1.5 W/cm² was selected as the test data set, and the complete data sequence collected at 2 W/cm² was used to validate the best individuals at the end of the MOGA. This validation data set is the most non-linear, and the temperature range includes the normal human-body temperature, making the validation process more realistic.

Mathematically the employed ARX model can be described by:

$$\hat{T}_{ARX}(u[k]) = b_1 u_1[k] + \dots + b_i u_i[k] + \dots + b_d u_d[k] \quad (1)$$

where $\{b_i\}_{i=1}^d$ are the model parameters and $\{u_i[k]\}_{i=1}^d$ are

the model inputs at instant k . Note that the past lags of the estimated variable (T) are included in the possible inputs, turning this model autoregressive. The values of $\{b_i\}_{i=1}^d$ were determined using the linear least squares strategy.

A RBFNN is a three-layered neural network (NN) where the first layer is a set of inputs, which connects the NN to its environment. The second layer, the unique hidden layer, is a set of processing elements called neurons, which perform a non-linear transformation on the input data. At the last layer the outputs of the hidden layer are linearly combined to produce the overall output of the NN (Haykin, 1999). The input/output relation for a RBFNN is given by:

$$\hat{T}_{RBFNN}(u[k]) = b + \sum_{i=1}^n \alpha_i \varphi(\|u[k] - c_i\|) \quad (2)$$

where n is the number of neurons in the hidden layer, b is the bias term, $\|\cdot\|$ is a norm, in this work an Euclidean norm was employed, and $\{\varphi_i\}_{i=1}^n$ is a set of non-linear radial basis functions with centre at $\{c_i\}_{i=1}^n$. The basis functions are evaluated at points $u[k]$ and are weighted by $\{\alpha_i\}_{i=1}^n$ at the last layer. The basis functions used were of Gaussian type:

$$\varphi_i = e^{-\frac{1}{2\sigma_i^2} \|u[k] - c_i\|^2} \quad (3)$$

where $\{\sigma_i\}_{i=1}^n$ is the spread of the i^{th} function.

The manual selection of the appropriate inputs in the ARX case, or the appropriate choice of the inputs and number of neurons in the RBFNN case, is a hard task due to the enormous number of possible model configurations. To solve this problem a MOGA was employed. The MOGA is a bio-inspired algorithm, which performs a population-based search by employing operators inspired in the natural evolution, such as selection, crossover, and mutation. This algorithm minimises or maximises a number of problem-dependent features (objectives), having in mind the attainment of well-fitted and also feasible solutions. In order to reach reasonable solutions, the objectives should be defined as goals to be met. For each goal, a priority is assigned, which defines the relative importance of the related objective for the final individual application. At the end of a MOGA run, a set of best-fitted individuals is obtained, which are the ones that fulfil or almost fulfil most of the *a priori* defined goals. In this work, the MOGA was allowed to choose an appropriate set of inputs for the ARX models and an appropriate set of inputs and number of neurons for the RBFNN models.

The MOGA generates 200 generations of 100 individuals each (100 NN or 100 ARX). The crossover and mutation probabilities are the same for both the ARX and RBFNN cases, and were defined as 0.7 and 0.5, respectively. These MOGA parameters were selected after several tests considering other parameters arrangements. The search space was delimited by defining: the possible number of neurons in the RBFNN case, and the possible number of inputs and the maximum lag (MLAG) considered for the input variables, for both ARX and RBFNN structure selection. The number of NN neurons and the number of inputs were defined as a number in the interval [2, 20], and the value of MLAG was defined as 20. These values were selected after several tests considering other possibilities.

As previously said, the ARX parameters were determined using the linear least-squares strategy. On the other hand, the RBFNN non-linear parameters (centres and spreads) were found using the Levenberg Marquardt (LM) algorithm, which is recognised as the best method for non-linear least-squares problems (Ruano *et al.*, 1992), which is the case of RBFNN training. The linear parameters of the NN (bias and weights) were also determined using the linear least-squares method. The initial value of the centres and spreads were found using a clustering algorithm, in this work the optimal adaptive *k*-means algorithm was used (Chinrungrueng and Séquin, 1995). To stop the neural networks training, the “early-stopping” criterion was used. This termination criterion accesses the model generalisation performance at each iteration of the training algorithm, and stops the training when this performance deteriorates, preventing model over-training (*i.e.* NNs which models the noise and are only specialised in the training data), being recognised as the optimal termination criterion for real-world applications (Principe *et al.*, 2000).

At each MOGA iteration (generation), and after the training, the performance of each model was accessed having in mind the extraction of objectives to minimise, and consequently to rank the individuals, improving the selection and reproduction of the best fitted. For the ARX models, the following measures were computed:

- Root mean square error in the training set – $RMSE_{TR}$;
- Root mean square error in the test set – $RMSE_{TE}$;
- Maximum root mean square error in all the prediction steps – MPE;
- Model-validity tests;
- Linear parameters norm – LPN.

For the RBFNN case the same measures were computed, in addition, the model complexity (MC) was included. Given the non-linear behaviour, the complexity of the RBFNN tends to reach very high values, compromising the model feasibility in a real-world environment. The choice of discarding this measure from the ARX selection procedure was due the fact that its complexity is the number of inputs, being 20 in the maximum, which is a very low value.

The model validity tests are explained in Billings and Voon (1986), and used in Teixeira *et al.* (2005) and Teixeira *et al.* (2006). These model validity tests involve the computation of first and higher order correlations between model inputs, outputs and residuals. In this work, as in Teixeira *et al.* (2005) and Teixeira *et al.* (2006), only the conditions involving the first order correlations were used, because the results obtained using the higher order correlations were not better in the RBFNN case, and it does not make sense to apply high order correlations to ARX models (linear models). The first-order correlations used were:

$$R_{ee}(\tau) = \delta(\tau) \quad (4)$$

$$R_{ue}(\tau) = 0 \forall \tau \quad (5)$$

where $R_{ee}(\cdot)$ is the auto-correlation of the error sequence, $R_{ue}(\cdot)$ is the cross-correlation between inputs and the error, $\delta(\cdot)$ is the Dirac's delta function, and τ is the time-shift or lag parameter associated with the correlation functions. In fact, $R_{ue}(\cdot)$ will never be precisely zero for all lags, in this way the equality is considered true if the normalised value of $R_{ue}(\cdot)$ lies within the 95% confidence limits defined as:

$$CI = \frac{1.96}{\sqrt{N}} \quad (6)$$

where N is the number of training patterns. In the same way, the value of $R_{ee}(\cdot)$ never equals the delta function, but the condition is considered true if the normalised value of the error auto-correlation enters the 95% confidence limit before lag one.

The NNs complexity (*MC*) was computed as the total number of parameters for a particular structure:

$$MC = NC \times NE + NS + NW \quad (7)$$

where NC is the number of centres, NE is the number of inputs, NS is the number of spreads, and NW is the number of linear weights.

An efficient model structure selection requires the minimisation of the previously defined model

measures. The MOGA was assigned to return, if possible, models which fulfil both the goals defined for the model measures. In order to perform a trustworthy comparison, the same goal values and priorities were defined for the ARX and RBFNN structure selection, with exception of the MC, which is only defined for the NNs. The $RMSE_{TR}$ was defined as a goal with value 0.004 (normalised value) and priority 1. In order to promote the selection of models with a high generalisation capacity, $RMSE_{TE}$ and MPE were defined as goals with priority 2 and values 0.002 and 0.003 (normalised values), respectively. The maximum of the correlation tests were defined with a goal value of $CI = 0.074$, and with priority 1. Models with a high LPN usually are too specialised in the training data, and when considering other data sets tend to have an exacerbated error, thus the LPN was defined as a goal with value 2.0 and priority 1. This value was defined based on the maximum number of NN neurons and in the data normalisation employed. The complexity of the NNs was defined as a goal with priority 1 and value 100. This goal value was defined having in mind the search space defined.

Results

ARX

The application of MOGA to the ARX models returned one preferable individual (PI). This individual was tested in the validation data (in this work the data collected at 2 W/cm^2), and a maximum absolute error of $2.08 \text{ }^\circ\text{C}$ was obtained. The minimum, average, and mean squared error obtained for this individual was: $-0.97 \text{ }^\circ\text{C}$, $0.22 \text{ }^\circ\text{C}$ and $0.38 \text{ } (^\circ\text{C})^2$, respectively. The inputs assigned by the MOGA to this PI are presented in Table 2.

The predicted temperature waveform in comparison with the measured one is presented in Figure 3a, the error signal is presented in Figure 3b, and the error distribution is presented in Figure 3c.

The performance of the best individual from the MOGA point of view is summarised in Table 3.

RBFNN

The application of MOGA to the RBFNN models held a

set of 18 preferable individuals (PI). As in the ARX case, the PIs were tested in the validation data. Afterwards, the maximum absolute error in the total validation sequence was computed, and the best individual selected as the one with the lowest maximum absolute predictive error.

The selected individual has 9 neurons, and presents a maximum absolute error of $0.42 \text{ }^\circ\text{C}$, a maximum error of $0.26 \text{ }^\circ\text{C}$, a minimum error of $-0.42 \text{ }^\circ\text{C}$, an average error of $-0.020 \text{ }^\circ\text{C}$, and a mean squared error of $0.0082 \text{ } (^\circ\text{C})^2$.

The inputs of this individual are presented in Table 4.

The predicted temperature waveform in comparison with the measured one is presented in Figure 4a, the error signal, as well as its average, maximum and minimum values are presented in Figure 4b. In Figure 4c the normalised error distribution is presented.

The properties of the best RBFNN model, from the MOGA point of view are presented in Table 5.

Discussion

Analysing Figures 3 and 4, it can be said that, for the conditions of this work, RBFNN predicts the temperature non-invasively in the glycerine medium with an error much smaller than the best obtained ARX model. Precisely, the maximum absolute error value attained for the RBFNN is approximately five times smaller than the error value obtained with the best ARX model. In addition, the maximum absolute error for the RBFNN is below $0.5 \text{ }^\circ\text{C}$, which is the value pointed as the borderline between an appropriate and an undesired temperature estimator. Given this threshold value, one can say that the best ARX model is an undesired estimator for single point and non-invasive temperature estimation in the modelling conditions applied. In terms of average error, the value attained for the best neural network is approximately one order of magnitude smaller than the value attained for the autoregressive models, indicating that the ARX models produce a more biased estimate than the RBFNN. This fact can also be seen in Figures 3c and 4c, where the error distribution is presented for both the best models. These figures show also that the

Table 2. Inputs of the best ARX model expressed as lags of the extracted features and lags of the temperature signal.

Lags of							
AF_{TUS}	$AH1_{TUS}$	$AH2_{TUS}$	A_{IUS}	BW_{IUS}	F_{IUS}	TP	T
0, 17	0, 5, 14	-	0, 2, 3, 19	1, 5, 11, 18	0, 11, 13, 17	5	2, 4

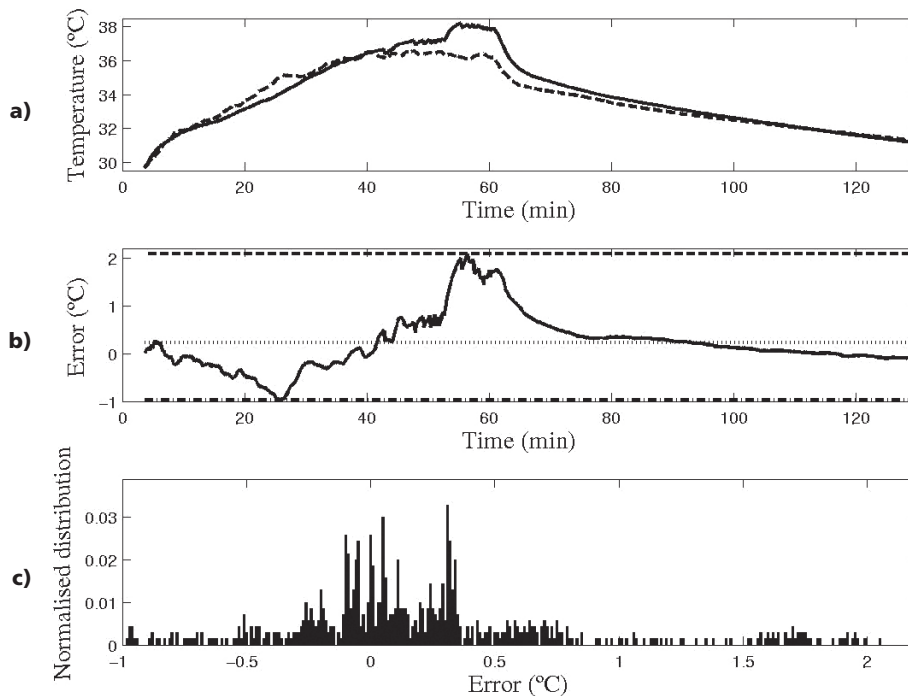


Figure 3. Performance of the best ARX model in the validation data; a) measured (solid line) and predicted temperature (dashed line); b) Error signal (solid line) and its maximum (dashed line), minimum (dash-dot line), and average (dotted line) values; c) Normalised error distribution.

Table 3. Characteristics of the best ARX model as compared to the *a priori* defined MOGA goals.

	RMSE _{TR}	RMSE _{TE}	MPE	LPN	R _{ee}	R _{ue}
Obtained	0.0011	0.00099	0.0031	6.68	0.053	0.10
Goal	0.004	0.0020	0.0030	2.0	0.074	0.074
Priority	1	2	2	1	1	1

Table 4. Inputs of the best RBFNN model expressed as lags of the extracted features and lags of the temperature signal.

Lags of							
AF _{TUS}	AH1 _{TUS}	AH2 _{TUS}	A _{IUS}	BW _{IUS}	F _{IUS}	TP	T
-	3	4, 6	0, 4, 14	16	13	5	4, 13, 19

estimate variance in the RBFNN case is smaller than in the ARX case, as expected. More precisely, the error committed by the RBFNN is practically all contained in the interval $[-0.1 \text{ } ^\circ\text{C}, 0.1 \text{ } ^\circ\text{C}]$. On the other hand, the error shown by the best ARX is practically all contained in the interval $[-0.5 \text{ } ^\circ\text{C}, 0.5 \text{ } ^\circ\text{C}]$.

As presented in Table 2, the best ARX has 20 inputs, which are pre-defined as the maximum number of inputs. Looking at this table, one can see the presence of short-term lags of the extracted features (AF_{TUS}(k),

AH1_{TUS}(k), AH1_{TUS}(k-5), etc.) and of the temperature (T(k-2), T(k-4)), and also long-term lags of the extracted features (AF_{TUS}(k-17), A_{IUS}(k-19), F_{IUS}(k-17)). Analysing Table 4 one can see that the best RBFNN has 12 inputs, that is 6 inputs less than for the ARX, which shows that the non-linear model needs less input information, through an increase in the processing capacity (complexity). The presence of short-term (AH1_{TUS}(k-3), AH2_{TUS}(k-4), AH2_{TUS}(k-6), TP(k-5), etc.) and long-term (A_{IUS}(k-14), BW_{IUS}(k-16), F_{IUS}(k-13)) lags of the extracted

features are present. The estimated temperature (T) contributes with one short-term lag ($T(k-4)$) and with two long-term lags ($T(k-13)$ and $T(k-19)$). Looking at the two input tables, it can be realised that the lag 20 never appears, showing that the value chosen for MLAG is sufficient to attain accurate temperature predictors.

In Table 3, the performance of the best ARX from the MOGA point of view is presented. Comparing the values obtained with the *a priori* defined goals it can be said that the best ARX fulfils 3 out of 6 goals. This model fulfils the goal defined for $RMSE_{TR}$, $RMSE_{TE}$ and R_{ee} , but not the most important one, which is the value defined for MPE, given that accurate temperature predictors are desired. The goal values defined for the linear parameters norm (LPN) and R_{ee} were not

fulfilled either and the obtained values are distant from the goal values.

In Table 5 the performance of the best RBFNN from the MOGA perspective is presented. This model fulfils 5 out of 7 goals. The ones not fulfilled are the MC and R_{ue} . Although these goals were not fulfilled the obtained values are close to the *a priori* defined values. In addition, this model fulfils the high priority goals ($RMSE_{TE}$ and MPE), showing its appropriateness for non-invasive temperature estimation in the applied experimental conditions.

Beyond the attained precision, the fundamental merit of this work lies on the alternative methodology employed. Both the models parameters and structure were extracted from the data, *i.e.* data-driven models.

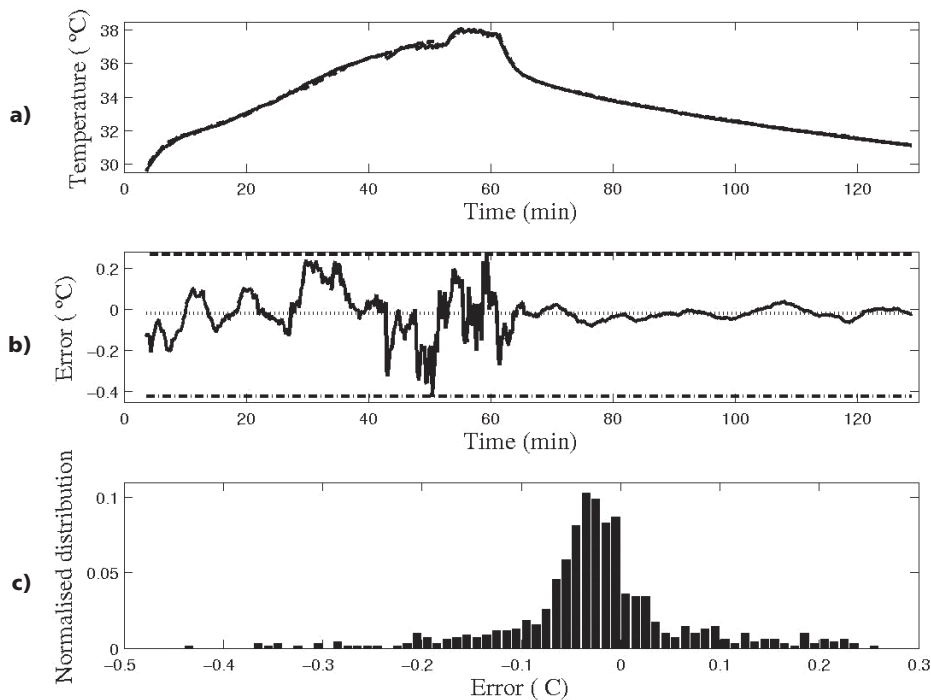


Figure 4. Performance of the best RBFNN model in the validation data; a) measured (solid line) and predicted temperature (dashed line); b) Error signal (solid line) and its maximum (dashed line), minimum (dash-dot line), and average (dotted line) values; c) Normalised error distribution.

Table 5. Characteristics of the best RBFNN model as compared to the *a priori* defined MOGA goals.

	$RMSE_{TR}$	$RMSE_{TE}$	MPE	LPN	R_{ee}	R_{ue}	MC
Obtained	0.00090	0.0010	0.0024	1.61	0.074	0.075	127
Goal	0.004	0.0020	0.0030	2.0	0.074	0.074	100
Priority	1	2	2	1	1	1	1

This means that mathematical simplifications and physical constant determination were discarded. This work presents alternative models which out-perform, in terms of precision, published empirical models. For example in the work of Seip and Ebbini (1995) a standard deviation of the error of 0.4 °C is presented, while the best RBFNN presents a standard deviation of the error of 0.09 °C. One of the limitations presented in Seip and Ebbini (1995) is the assumption that temperature is linear with the spectral components of the echoes, for temperature changes below 10 °C. The non-linear and data-driven behaviour of the RBFNN models hereby presented, can probably overcome these limitations.

Given the non-invasive and recursive behaviour of the estimators, one question that arises is the initial temperature definition. Both model types (ARX and RBFNN) were tested by furnishing them an initial temperature with 1 °C difference around the correct value, and it was observed that the error of both model types converge to the one obtained with the correct initial temperature. In fact, for the best RBFNN this error is below 0.5 °C after 4 min. This means that probably, in an *in vivo* application, an initial temperature of 37 °C can be considered, given that well-trained models can cancel initial temperature errors.

Conclusions

The work presented in this paper compares two modelling strategies for non-invasive single-point temperature prediction in a homogeneous medium. The two compared strategies were an autoregressive model with exogenous inputs (linear model) and radial basis functions neural network (non-linear model). The obtained results show that the relation between the extracted RF-lines features and the temperature of the medium is essentially non-linear, once the performance obtained with the best RBFNN was clearly superior to the linear (ARX) approach. The best RBFNN presents a maximum absolute predictive error five times smaller than the best ARX model. In addition it needs less information from the environment, given the reduction on the number of inputs.

The results obtained are encouraging for the application of the RBFNN in multi-layered media, and subsequently in *in vivo* applications. In the future, a spatial modelling with a resolution of 1 cm³ and maximum absolute error less than 0.5 °C, using these neural networks, must be investigated.

Acknowledgements

The authors would like to acknowledge the financial

support of: Fundação para a Ciência e a Tecnologia (grant SFRH/BD/14061/2003), Portugal, and Conselho Nacional de Desenvolvimento Científico e Tecnológico (CNPq/CYTED/490.013/03-1), Brazil. The authors acknowledge also the help of Prof. Hector Gomez and MSc Guillermo Cortela in the experimental setup.

References

- Arthur, R.M., Straube, W.L., Trobaugh, J.W., Moros, E.G. (2005), "Non-invasive estimation of hyperthermia temperatures with ultrasound", *International Journal of Hyperthermia*, v. 21, n. 6, p. 589-600.
- Billings, S., Voon, W. (1986), "Correlation based model validity tests for non-linear models", *International Journal of Control*, v. 44, p. 235-244.
- Chinrungrueng, C., Séquin, C.H. (1995), "Optimal adaptive k-means algorithm with dynamic adjustment of learning rate", *IEEE Transactions on Neural Networks*, v. 6, n. 1, p. 157-169.
- Fonseca, C.M., Fleming, P.J. (1993), "Genetic algorithms for multi-objective optimization: formulation, discussion and generalization", In: *Proceedings of the 5th International Conference on Genetic Algorithms*, Urbana-Champaign, p. 416-423, June.
- Haykin, S. (1999), *Neural Networks: A Comprehensive Foundation*, New Jersey: Prentice Hall.
- Hynynen, K., Chung, A., Fjield, T., Buchanan, M., Daum, D., Colucci, V., Lopath, P., Jolesz, F. (1996), "Feasibility of using ultrasound phased arrays for MRI monitored noninvasive surgery", *IEEE Transactions on Ultrasonics Ferroelectrics and Frequency Control*, v. 43, n. 6, p. 1043-1053.
- Meaney, P.M., Paulsen, K.D., Hartov, A., Crane, R.K. (1996), "Microwave imaging for tissue assessment: initial evaluation in multitarget tissue-equivalent phantoms", *IEEE Transactions on Biomedical Engineering*, v. 43, n. 9, p. 878-890.
- Paulsen, K.D., Moskowitz, M.J., Ryan, T.P., Mitchell, S.E., Hoopes, P.J. (1996), "Initial *in vivo* experience with EIT as a thermal estimator during hyperthermia", *International Journal of Hyperthermia*, v. 12, n. 5, p. 573-591.
- Principe, J.C., Euliano, N.R., Lefebvre, W.C. (2000), *Neural and Adaptive Systems: Fundamentals Through Simulations*, New York: John Wiley & Sons.
- Ruano, A.E.B., Fleming, P.J., Jones, D.I. (1992), "Connectionist approach to PID autotuning", *IEE Proceedings*, v. 139, n. 3, p. 279-285.
- Seip, R., Ebbini, E.S. (1995), "Noninvasive estimation of tissue temperature response to heating fields using diagnostic ultrasound", *IEEE Transactions on Biomedical Engineering*, v. 42, n. 8, p. 828-839.
- Simon, C., VanBaren, P., Ebbini, E.S. (1998), "Two-dimensional temperature estimation using diagnostic ultrasound", *Transactions on Ultrasonics Ferroelectrics and Frequency Control*, v. 45, n. 4, p. 1088-1099.
- Teixeira, C.A., Cortela, G., Gomez, H., Ruano, M.G., Ruano, A.E., Negreira, C., Pereira, W.C.A. (2004), "Temperature models of a homogeneous medium under therapeutic ultrasound", *IFMBE Newsletter*, v. 69, p. 52-56.

- Teixeira, C.A., Ruano, A.E., Negreira, C., Ruano, M.G., Pereira, W.C.A. (2005), "Neural network model for non-invasive two-point temperature monitoring in a homogeneous medium irradiated by therapeutic ultrasound", In: *IFMBE Proceedings of the 3rd European Medical & Biological Engineering Conference, [EMBEC'05]*, Prague, v. 11, (CDROM), 20-25 Nov.
- Teixeira, C.A., Ruano, A.E., Ruano, M.G., Pereira, W.C.A., Negreira, C. (2006), "Non-invasive temperature prediction of in vitro therapeutic ultrasound signals using neural networks", *Medical and Biological Engineering & Computing* (in press).
- Ter Haar, G. (1999), "Therapeutic ultrasound", *European Journal of Ultrasound*, v. 9, n. 1, p. 3-9.
- Ueno, S., Hashimoto, M., Fukukita, H., Yano, T. (1990), "Ultrasound thermometry in hyperthermia", In: *Proceedings of the IEEE Ultrasonic Symposium*, Honolulu, v. 3, p. 1645-1652, 04-07 Dec.

